

# Abrupt transitions in high-concentration, particle-driven gravity currents

Mark A. Hallworth<sup>a)</sup> and Herbert E. Huppert<sup>b)</sup>

*Institute of Theoretical Geophysics, Department of Applied Mathematics and Theoretical Physics,  
University of Cambridge, Cambridge CB3 9EW, United Kingdom*

(Received 19 August 1997; accepted 28 January 1998)

A systematic series of experiments on the instantaneous release of two-dimensional, heavy, particle-driven gravity currents has been conducted. High-concentration currents propagated in a qualitatively different way than low concentration currents. In particular, beyond a critical initial volume fraction of particles, the resulting dense current came to an abrupt halt at some point down the channel, depositing the bulk of its initial sediment load as a relatively thick layer of fairly constant thickness, characterized by a pronounced, steep snout. A very much thinner layer of sediment extended for some distance beyond the arrest point. This layer was deposited from the subsequent propagation of a slower moving, low concentration residual cloud. © 1998 American Institute of Physics. [S1070-6631(98)01505-0]

## I. INTRODUCTION

Gravity currents, which occur whenever fluid of one density flows primarily horizontally into fluid of a different density, are driven by the excess buoyancy between the intruding fluid and the ambient. Particle-driven gravity currents derive their buoyancy force from the bulk density excess due to the presence of suspended particles, and occur in numerous man-made and natural situations. Examples include the discharge of effluent and industrial waste into rivers or coastal waters, turbidity currents in ocean basins, pyroclastic flows from volcanic eruptions, mudflows and snow avalanches, along with the laboratory simulations of many of these flows. Understanding the propagation of such flows is an important factor in studies of pollutant dispersion and the evaluation of natural hazard assessment.

A fundamental feature of suspension flows is that the particles, which are generally more dense than the transporting fluid, continually separate from the flow through sedimentation, thereby modifying the concentration in both space and time. Some of the effects associated with the propagation of particle-driven gravity currents have recently been analyzed, yielding both numerical and analytical solutions for the finite run-out distance of particle-driven currents and the final distribution of sedimented material.<sup>1-4</sup> Many of the results have been confirmed by laboratory experiments, as discussed in these papers. All these studies, however, have focused on currents with relatively low initial volume concentrations of particles  $\phi_0$ , (typically  $\phi_0 \approx 10^{-2}$ ). The aim of this letter is to present the results of a new series of one-dimensional laboratory experiments on fixed-volume suspension flows in which the initial volume concentration of (heavy) particles was gradually increased to values approaching the maximum that could be fluidized ( $\phi_0 \approx 0.45$ ). It was found that very high concentration “slurries” behave quite differently from low-concentration flows,

and their propagation is inadequately described by the previous theoretical models cited above. The main new phenomenon described is that suspensions with initial volume fractions larger than  $\approx 0.3$  propagate as rapidly moving, densely-compacted currents, but are marked by a pronounced and sudden arrest. The arrest becomes progressively closer to the release point as the initial volume fraction is increased. Turbulent mixing along the upper surface of the dense flow prior to arrest generates a diffuse, low-concentration overlying cloud which subsequently advances beyond the point of arrest, but this only accounts for a very small fraction of the initial mass loading. The abrupt transition is reflected in the final sedimented deposit on the floor, which displays an almost discontinuous step at the point of transition. Unfortunately, this letter does not present a quantitative explanation of the observed phenomena, as useful as that would be. Despite many discussions with colleagues, we are still unsure of the physical causes behind the effects we present here, and do so to stimulate further investigation.

## II. EXPERIMENTS

The experiments all involved the instantaneous release of fixed volumes of particle/water suspensions, initially held behind a lock gate positioned near one end of a long rectangular channel filled with water to a depth  $H$ , as depicted in Fig. 1. Two different experimental channels were used: one measuring 100 cm long, 15 cm wide and 10 cm deep; and the other measuring 200 cm long, 20 cm wide and 25 cm deep. In both channels, the lock length,  $x_0$ , was held fixed at 3 cm. The suspensions used were made by mixing fairly monodisperse, non-cohesive silicon carbide particles in water behind the gate. Details of the particle size distributions and tracings of representative particle shapes are given in Huppert *et al.*<sup>5</sup> The initial mixing was achieved using a mechanical stirrer, and became progressively more difficult as the volume fraction of particles increased. However, once a uniform suspension was attained, it could subsequently be maintained with only relatively minor agitation. The particles have a density

<sup>a)</sup>Electronic mail: hallworth@esc.cam.ac.uk

<sup>b)</sup>Electronic mail: heh1@esc.cam.ac.uk

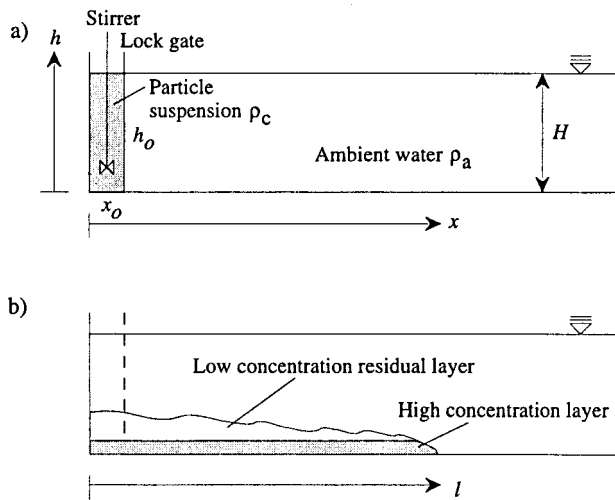


FIG. 1. Schematics of (a) the experimental setup and starting configuration, and (b) the structure of the flow at some time  $t > 0$ .

$\rho_p$  of  $3.217 \text{ g cm}^{-3}$ , and five different size grades were used, having mean particle diameters  $d$  of 9, 17, 23, 37 and  $53 \mu\text{m}$ . The total mass of solids initially suspended,  $M_0$ , varied between 10 and 724 g, yielding a range of initial volume fractions  $\phi_0$  from 0.009 to 0.432, calculated from

$$\phi_0 = \frac{M_0}{\rho_p A_0 w}, \quad (1)$$

where  $A_0 = x_0 h_0$  is the initial cross-sectional area of suspension behind the lock and  $w$  is the tank width. The density of the current,  $\rho_c$ , is given by

$$\rho_c = \phi \rho_p + (1 - \phi) \rho_a, \quad (2)$$

where  $\rho_a$  is the density of the ambient fluid. The reduced gravity of the current,  $g'$ , is then defined by

$$g' = \frac{g(\rho_c - \rho_a)}{\rho_a} \quad (3a)$$

$$= g'_p \phi, \quad (3b)$$

where  $g$  is the gravitational acceleration, and  $g'_p = g(\rho_p - \rho_a)/\rho_a$  is the reduced gravity of the particles. The experiments described here give a range of values of  $\rho_c$  from 1.019 to  $1.957 \text{ g cm}^{-3}$ , and initial values of the reduced gravity  $g'$  from 18.8 to  $939 \text{ cm s}^{-2}$ . A full listing of the experiments and their initial conditions is presented in Table I.

The currents were initiated by rapid vertical withdrawal of the lock gate, allowing the dense particle suspension to collapse and flow across the base of the tank. Each experimental run was recorded on videotape, and measurements of the position of the flowfront,  $l$ , as a function of time were extracted from slow-motion replays. In some experiments (particularly those conducted in the 1 m long tank), the current hit the far end wall and was reflected, but only data prior to rebound was recorded. Once all the particles had settled out, their distribution over the channel floor was measured by sampling the mass of particles per unit area,  $D$ , as a function of distance from the release point. Sediment sampling was only attempted following experiments in the 2 m

long tank in those cases where the current terminated before reaching the end wall, and was achieved by vacuuming-up the sediment within a narrow strip of known area across the width of the tank using a siphon tube, at various positions along the sediment layer. The particles were collected in a beaker, then dried and weighed to yield the mass of deposit per unit area. As a check on the sampling method, the total mass of sediment could be calculated by integrating the measured deposit profile. The recovered value was always within 2% of the actual initial mass of particles in suspension, thus confirming the accuracy of the technique.

### III. RESULTS

#### A. The effect of particle concentration

The abrupt arrest observed for high-concentration, particle-driven gravity currents is illustrated most effectively by considering the rate of propagation of the flowfront for a series of experiments in which the initial volume fraction of particles is systematically increased. A plot of distance as a function of time for such a series using  $9 \mu\text{m}$  particles is presented in Fig. 2(a). At the lowest concentration ( $\phi_0 = 0.025$ ), the velocity of the flowfront decreases smoothly with distance, and the experimental data agrees well with both analytical and numerical predictions. An increase in the initial concentration to  $\phi_0 = 0.15$  is accompanied by a corresponding increase in velocity. However, the coincidence of data points for experiments with values of  $\phi_0$  of 0.15, 0.25 and 0.275 implies that some maximum velocity is attained within this medium concentration regime, irrespective of  $\phi_0$  and hence  $g'_0$ . This is in conflict with the predictions of any theoretical model known to us. The data for experiments with  $0.275 < \phi_0 < 0.40$  initially follow the maximum velocity curve, but all show a point of deviation, which becomes progressively closer to the source as the initial volume fraction of particles is increased. The deviation point identifies the position at which the dense current was observed visually to be abruptly arrested. Subsequent data points correspond to the much slower, forward propagation of a low concentration, residual particle suspension generated by turbulent mixing along the upper surface of the current during the initial rapid advance.

The abrupt transition is also clearly reflected in the form of the final sedimented layer. Figure 2(b) plots the measured deposit density as a function of distance from the source, for the experimental series using the  $9 \mu\text{m}$  particles described above. The deposit densities have been normalized by the initial mass loading,  $M_0$ , and thus the integrated profiles or areas below each curve are identical. For  $\phi_0 = 0.025$ , the profile is typical of that deposited from low-concentration suspensions (Bonnecaze *et al.*,<sup>1</sup> Fig. 13), and shows a slight downstream maximum before decreasing asymptotically to zero. For  $\phi_0 = 0.15$ , the profile becomes flattened and extends to a larger value of  $x$ . With further increases in  $\phi_0$ , the profiles develop a step which becomes both progressively steeper and closer to the source. Furthermore, a trough develops in the sediment layer at a distance of approximately 20 cm, which deepens as  $\phi_0$  increases.

TABLE I. The initial conditions of the various particle-driven gravity currents, arranged by particle size and then in ascending order of the initial volume fraction of particles. Runs prefixed by the letter A were conducted in the 1 m long tank ( $w=15$  cm): those prefixed by the letter B in the 2 m long tank ( $w=20$  cm). The distribution of particles in the final sedimented layer was measured for runs marked with an asterisk. The values of  $g'$  and  $g''$  were calculated using Equations (3) and (9), respectively.

Run	$d$ ( $\mu\text{m}$ )	$x_0$ (cm)	$h_0$ (cm)	$A_0$ ( $\text{cm}^2$ )	$M_0$ (g)	$\phi_0$	$\rho_c$ ( $\text{g cm}^{-3}$ )	$g'$ ( $\text{cm s}^{-2}$ )	$g''$ ( $\text{cm s}^{-2}$ )
A20	9	3.0	8.0	24.0	10.0	0.009	1.019	18.8	18.4
B28*	9	3.0	10.0	30.0	48.3	0.025	1.055	54.4	51.6
A21	9	3.0	8.0	24.0	100.0	0.086	1.191	187.8	157.6
B40*	9	3.0	10.0	30.0	289.5	0.150	1.333	326.2	244.8
A22	9	3.0	8.0	24.0	200.0	0.173	1.383	375.6	271.6
B29*	9	3.0	10.0	30.0	482.5	0.250	1.554	543.7	349.8
A23	9	3.0	8.0	24.0	300.0	0.259	1.574	563.4	357.9
B43*	9	3.0	10.0	30.0	530.8	0.275	1.610	598.1	371.6
A26	9	3.0	8.0	24.0	330.0	0.285	1.632	619.7	379.8
B38*	9	3.0	10.0	30.0	579.1	0.300	1.665	652.6	391.9
A27	9	3.0	8.0	24.0	367.0	0.317	1.703	689.2	404.8
B42*	9	3.0	10.0	30.0	627.3	0.325	1.721	706.8	410.8
A24	9	3.0	8.0	24.0	400.0	0.345	1.766	751.2	425.4
B30*	9	3.0	10.0	30.0	675.6	0.350	1.776	761.2	428.6
B41*	9	3.0	10.0	30.0	723.8	0.375	1.831	815.6	445.3
B39*	9	3.0	10.0	30.0	772.1	0.400	1.887	870.0	461.1
A25	9	3.0	8.0	24.0	500.0	0.432	1.957	939.0	479.8
B34*	17	3.0	10.0	30.0	675.6	0.350	1.776	761.2	428.6
A1	23	3.0	8.0	24.0	10.0	0.009	1.019	18.8	18.4
A4	23	3.0	8.0	24.0	100.0	0.086	1.191	187.8	157.6
A3	23	3.0	8.0	24.0	200.0	0.173	1.383	375.6	271.6
A7	23	3.0	8.0	24.0	281.0	0.243	1.538	527.7	343.1
A5	23	3.0	8.0	24.0	400.0	0.345	1.766	751.2	425.4
A2	23	3.0	8.0	24.0	500.0	0.432	1.957	939.0	479.8
A14	37	3.0	8.0	24	10.0	0.009	1.019	18.8	18.4
B31*	37	3.0	10.0	30.0	48.3	0.025	1.055	54.4	51.6
A15	37	3.0	8.0	24.0	100.0	0.086	1.191	187.8	157.6
A16	37	3.0	8.0	24.0	200.0	0.173	1.383	375.6	271.6
B32*	37	3.0	10.0	30.0	482.5	0.250	1.554	543.7	349.8
A17	37	3.0	8.0	24.0	300.0	0.259	1.574	563.4	357.9
A18	37	3.0	8.0	24.0	400.0	0.345	1.766	751.2	425.4
B33*	37	3.0	10.0	30.0	675.6	0.350	1.776	761.2	428.6
A19	37	3.0	8.0	24.0	500.0	0.432	1.957	939.0	479.8
A8	53	3.0	8.0	24.0	10.0	0.009	1.019	18.8	18.4
A9	53	3.0	8.0	24.0	100.0	0.086	1.191	187.8	157.6
A10	53	3.0	8.0	24.0	200.0	0.173	1.383	375.6	271.6
A11	53	3.0	8.0	24.0	300.0	0.259	1.574	563.4	357.9
A12	53	3.0	8.0	24.0	400.0	0.345	1.766	751.2	425.4
B37*	53	3.0	10.0	30.0	675.6	0.350	1.776	761.2	428.6
A13	53	3.0	8.0	24.0	500.0	0.432	1.957	939.0	479.8

## B. The effect of particle size

In Fig. 3, results are presented for a series of experiments in which the initial volume concentration of particles was fixed at  $\phi_0=0.35$ , but the particle diameter was varied between 9 and 53  $\mu\text{m}$ . The plot of distance as a function of time [Fig. 3(a)] reveals deviation points that mark the sudden arrest which are more or less coincident for each of the four different particle sizes used, all occurring at approximately 75 cm. In addition, the deposit density data shown in Fig. 3(b) depicts the arrested snout of the sedimented layer becoming progressively steeper as the particle size decreases. The profile for the 53  $\mu\text{m}$  particles exhibits a fairly steady

decrease in deposit density between 50 and 100 cm, whereas the profile for the 9  $\mu\text{m}$  particles shows a rapid initial decrease between 0 and 20 cm, then levels out as a shoulder before steepening sharply at approximately 75 cm.

## IV. COMPARISON WITH PREVIOUS THEORETICAL MODELS

From the above description, it is clear that no theoretical approach already developed can account for and collapse the data. Nevertheless, it is beneficial to present a nondimensionalization of the data in order to compare experiments with

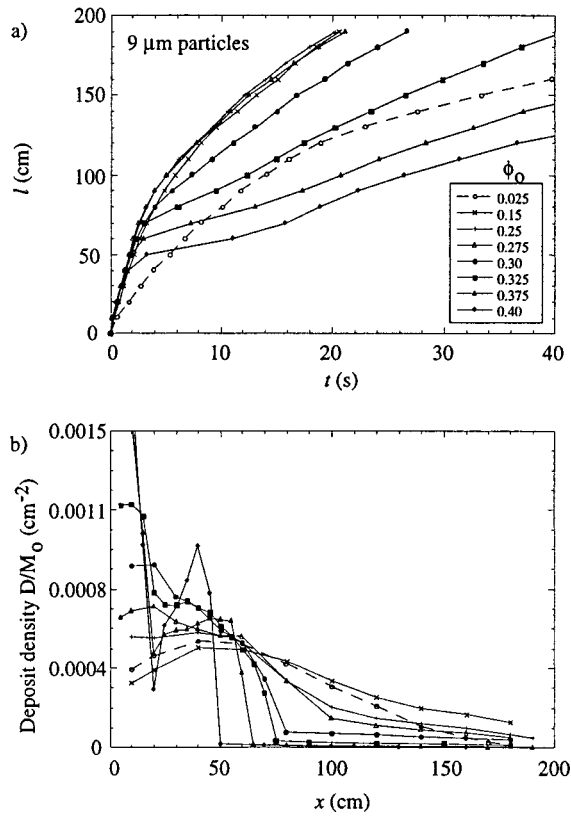


FIG. 2. Plots of (a) position of the flowfront as a function of time, and (b) deposit density as a function of distance for a series of gravity currents using 9  $\mu\text{m}$  particles and various initial volume fractions of particles, as indicated in the legend.

different starting conditions. Following the box model approach of Dade and Huppert,<sup>2</sup> Hallworth, Hogg and Huppert<sup>6</sup> introduced the nondimensional variables

$$\xi = l/l_\infty, \tag{4}$$

and

$$\tau = t/T, \tag{5}$$

for length and time respectively. The final run-out length of the current

$$l_\infty = 1.6(25\text{Fr}^2 g'_0 A_0^3 / V_s^2)^{1/5}, \tag{6}$$

and the time scale

$$T = \left( \frac{l_\infty^3}{\text{Fr}^2 g'_0 A_0} \right)^{1/2}, \tag{7}$$

where  $V_s$  is the Stokes' free fall velocity of the particles given by  $g'_p d^2 / 18\nu$ , and the Froude number of the flow  $\text{Fr}=1.19$  is constant. Hallworth *et al.*<sup>6</sup> developed an analytical relationship for dilute particle-driven gravity currents given by

$$\tau = \int_0^\xi \frac{s^{1/2} ds}{1-s^{5/2}} \equiv \mathcal{F}(\xi). \tag{8}$$

This relationship is plotted in Figure 4 along with the scaled data for the length of the current as a function of time from

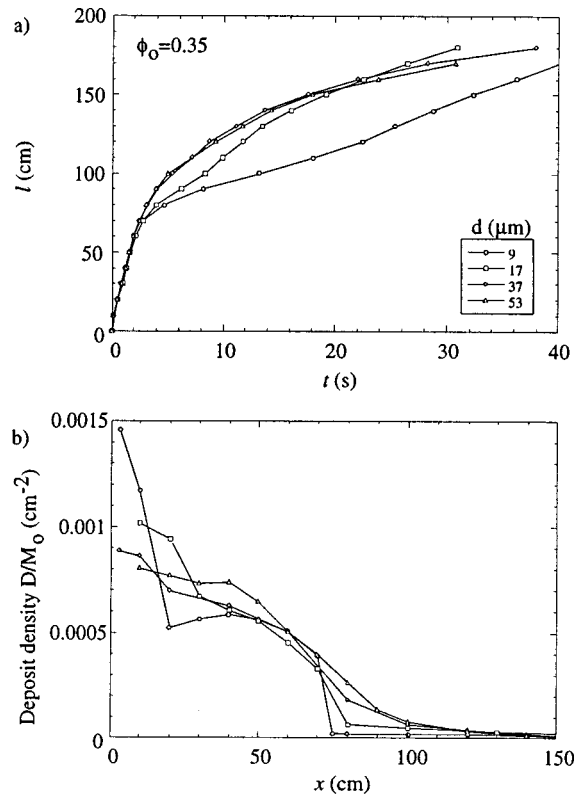


FIG. 3. Plots of (a) position of the flowfront as a function of time, and (b) deposit density as a function of distance for a series of gravity currents each with the same initial volume fraction of particles of  $\phi_0=0.35$ , but using particles with different mean diameters, as indicated by the legend.

selected experiments reported here. The data for low-concentration flows ( $\phi_0=0.086$ ) show excellent agreement with the theoretical curve. The scaled data for experiments at higher concentrations ( $\phi_0=0.35$  and  $0.43$ ) also show good agreement with the theoretical curve up to the point of arrest,

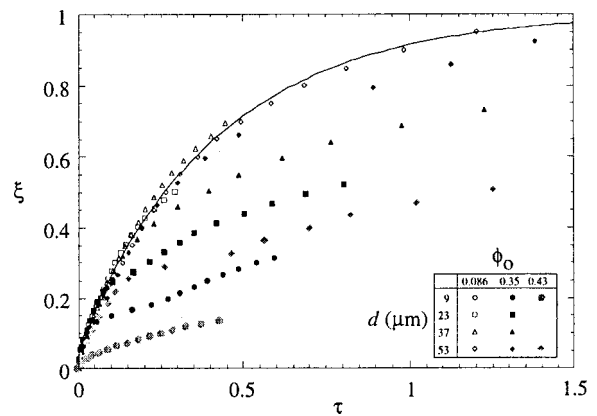


FIG. 4. Nondimensional length as a function of nondimensional time for selected particle-driven gravity currents with different initial volume fractions  $\phi_0$  and mean particle diameters  $d$ , as given in the legend. The theoretical relationship expressed by Equation (8) is shown as a solid curve. Currents with low initial volume concentrations ( $\phi_0=0.086$ ) agree well with the theoretical prediction. Those with high initial volume concentrations ( $\phi_0=0.35, 0.43$ ) show deviations from the theory which occur progressively closer to the source as  $\phi_0$  increases and  $d$  decreases.

but the arrest distance becomes an increasingly smaller fraction of the predicted run out distance as the volume fraction increases and the particle size decreases.

For dense currents with high  $\rho_c/\rho_a$  ratios, Gröbelbauer, Fannelop and Britter<sup>7</sup> have suggested that a better quantitative interpretation is obtained from a representation of the reduced gravity expressed by

$$g'' = \frac{g(\rho_c - \rho_a)}{\rho_c} \quad (9a)$$

$$= g_p'' \phi, \quad (9b)$$

where  $g_p'' = g(\rho_p - \rho_a)/\rho_c$ . Adopting this alternative representation instead of that given by (3) makes a negligible difference at low particle concentrations, but decreases the value of the reduced gravity by roughly half at the highest concentrations used in these experiments, as seen in Table I. Rescaling the data using  $g''$  rather than  $g'$  however, does not explicitly improve the comparison with the theory, and indicates that the use of  $g''$  is not sufficient to explain the different results at high concentrations.

## V. SUMMARY

The discrepancy between these new experimental results and the theoretical prediction for high-concentration flows is not meant to discredit the box model approach, which is based on the implicit assumption that  $\phi_0 \ll 1$ , and does not claim to be valid for high-concentration flows. The comparison is merely used as a convenient way of scaling the data and emphasizing the different regimes of behavior between low- and high-concentration currents. The data indicate that a critical value of the initial volume fraction of particles of  $\phi_0 \approx 0.275$  separates these two regimes. For particle-driven currents with initial volume fractions in the range  $0 < \phi_0 < 0.275$ , the final run out length of the sedimented deposit increases as  $\phi_0$  increases. Currents with initial volume frac-

tions in the range  $0.275 < \phi_0 < 0.45$  (the higher limit being the approximate maximum for fluidization), undergo an abrupt arrest, and the final run out length of the sediment layer *decreases* as  $\phi_0$  increases.

There are several industrial and natural situations in which particle-driven flows are initiated at both low and high particle concentrations. For example, turbidity currents, which transport clastic sediment from continental margins to deep ocean basins, may be generated by resuspension of sediment through turbulent bed erosion in shallow continental shelf environments, or by the catastrophic slumping of unconsolidated sediment on continental slopes. In the former case, the concentration of particles is low, and approaches its maximum value from zero. In the latter case, the current is initiated at the highest possible volume fraction following fluidization of close-packed sediment, as are many other debris flows generated by gravitational collapse. Our experiments indicate that theoretical attempts to predict the propagation of high-concentration particulate flows require a different approach to that which successfully describes low-concentration currents.

- <sup>1</sup>R. T. Bonnecaze, H. E. Huppert, and J. R. Lister, "Particle-driven gravity currents," *J. Fluid Mech.* **250**, 339 (1993).
- <sup>2</sup>W. B. Dade and H. E. Huppert, "Predicting the geometry of channelised deep-sea turbidites," *Geology* **22**, 645 (1994).
- <sup>3</sup>W. B. Dade and H. E. Huppert, "Runout and fine-sediment deposits of axisymmetric gravity currents," *J. Geophys. Res.* **100**, 18597 (1995).
- <sup>4</sup>R. T. Bonnecaze, M. A. Hallworth, H. E. Huppert, and J. R. Lister, "Axisymmetric particle-driven gravity currents," *J. Fluid Mech.* **294**, 93 (1995).
- <sup>5</sup>H. E. Huppert, R. C. Kerr, J. R. Lister, and J. S. Turner, "Convection and particle entrainment driven by differential sedimentation," *J. Fluid Mech.* **226**, 349 (1991).
- <sup>6</sup>M. A. Hallworth, A. J. Hogg, and H. E. Huppert, "Effects of external flow on compositional and particle gravity currents," *J. Fluid Mech.* **359**, 109 (1998).
- <sup>7</sup>H. P. Gröbelbauer, T. K. Fannelop, and R. E. Britter, "The propagation of intrusion fronts of high density ratios," *J. Fluid Mech.* **250**, 669 (1993).